Environmental life cycle assessment and techno-economic analysis of triboelectric nanogenerator

Abdelsalam Ahmed[1,2], Islam Hassan[2,3], Taofeeq Ibn-Mohammed[4,5], Ian M. Reaney[6], Lenny S.C. Koh[4,5], Heather MacLean[7], Jean Zu[2], Zhong Lin Wang[1,8*]

[1]School of Materials Science & Engineering, Georgia Institute of Technology, Atlanta, Georgia 30332-0245, USA
[2]NanoGenerators & NanoEngineering Laboratory, School of Mechanical & Industrial Engineering, University of Toronto, Toronto, M5S 3G8, Canada
[3]Design & Production Engineering Department, Faculty of Engineering, Ain Shams University, Cairo, 11535, Egypt
[4]Centre for Energy, Environment & Sustainability, The University of Sheffield, Sheffield, S10 1FL, UK
[5]Advanced Resource Efficiency Centre, The University of Sheffield, Sheffield, S10 1FL, UK
[6]Departments of Materials Science & Engineering, University of Sheffield, Sheffield, S1 3JD, UK
[7]School of Civil Engineering, University of Toronto, Toronto, M5S 3G8, Canada
[8]Beijing Institute of Nanoenergy & Nanosystems, Chinese Academy of Sciences, Beijing, 100083, China

Corresponding author: zu@mie.utoronto.ca

Abstract

As the world economy grows and industrialization of the developing countries increases, the demand for energy continues to rise. Triboelectric nanogenerators (TENGs) have been touted as having great potential for low-carbon, non-fossil fuel energy generation. Mechanical energies from, amongst others, body motion, vibration, wind and waves, are captured and converted by TENGs to harvest electricity, thereby minimizing global fossil fuel consumption. However, only by ascertaining the performance efficiency versus cost of materials and manufacture as well as their environmental profile in comparison with other energy harvesting technologies can the true potential of TENGs be established. This paper presents a detailed techno-economic lifecycle assessment of two representative examples of TENG modules, one with a high performance efficiency (Module A) and the other with a lower efficiency (Module B) both fabricated using low cost materials. The results are discussed across a number of sustainability metrics in the context of other energy harvesting technologies, notably photovoltaics. Module A possesses a better environmental profile, lower cost of production, lower CO_2 emissions and shorter energy payback period (EPBP) compared to Module B. However, the environmental profile of Module B is slightly degraded due to higher content of acrylic in its architecture and higher electrical energy consumption during fabrication. The end of life scenario of acrylic is environmentally viable given their recyclability and reuse potential and do not generate toxic gases that are harmful to humans and the environment during combustion processes due to its stability during exposure to ultraviolet radiation. Despite the adoption of a less optimum laboratory manufacturing route, TENG modules generally have a better environmental profile than commercialized Si based and organic solar cells, but Module B has a slightly higher energy payback period than PV technology

based on perovskite-structured methyl ammonium lead iodide. Overall, we conclude that future research in TENGs should focus on improving systems performance, materials optimization and more importantly lifespan to realize their full potential.

1. Introduction

The burning of fossil fuels is responsible for > 80% of primary energy demands and current profiles reveal that the world remains highly dependent on carbon-based power generation resulting in the emission of record levels of carbon dioxide (CO_2).[1] The growth of the world economy, coupled with industrialization of the developing world has resulted in a demand for energy that continues to increase.[2] Given the growing demand for energy and dwindling oil reserves, the development of alternative, sustainable energy is paramount. Energy from solar, wind and tidal waves have the potential to be integrated with the electrical power grids to meet mega- to gigawatt power requirements[3]. The overall requirements for harvesting these forms of energy are based on a number of factors including low-cost, high stability and high efficiency.[3]

An increasingly wide range of mobile electronic devices often connected to the Internet of Things (IoT) have not only modified our way of life but also created the need for a highly diversified energy platform.[3] For applications such as medical care, healthcare monitoring, infrastructure monitoring, environmental protection and security, many sensors, computer control circuits and antennas are required. Although the power for driving each miniature system is relatively small (from milli to micro-watt range)[3], the collective number of units is forecast by Cisco (the worldwide leader in information technology) to be in the trillions by the year 2020.[4] The use of batteries to power these units is currently the default solution but this is not sustainable given the large number required and their limited life span. Moreover, the concept of the IoT will be rendered meaningless without the inherent ability of devices to be self-powered. This challenge has prompted the development of nanogenerators that harvest mechanical energy from the surrounding environment. Nanogenerators were first developed based on two effects namely, piezoelectricity [5-10] and triboelectricity [11-13], with intention of harvesting energy from activities such as walking, talking, typing and breathing. A string of groundbreaking research advances have subsequently being reported since the landmark publications by Wang and Song.[14]

The concept of the triboelectric generator (TEG) or triboelectric nanogenerator (TENG) is based on the use of the electrostatic charges created on the surfaces of two dissimilar materials when they are brought into physical contact, the contact induced triboelectric charges can generate a potential drop when the two surfaces are separated by a mechanical force, causing the electrons to flow between the two electrodes built on the two surfaces.[3, 15] Since the first publication on TENG in 2012, huge progress has been recorded. For instance, by the year 2015, the area power density reached 500W/m^2, and the volume power density attained 15 MW/m^3, with an instantaneous conversion efficiency of around 70%.[16] TENGs boast a wide range of applications, given their capability to harvest mechanical energy from a variety of sources, including body motions, vibrations, wind and waves.[17] Additionally, the successful application of TENGs in self-powered chemical sensors current research has recently been demonstrated,[18-20] driving electrochemical processes[21-23] and commercial light-emitting diodes (LEDs).[24-27]

Several fabrication processes for TENGs have been described in the extant literature. Specifically, four modes of operations of TENG, including vertical contact-separation mode, in-plane sliding mode, single-electrode mode and free-standing triboelectric-layer mode were extensively described by Wang et al.[3] In this paper, attention is focused on two fabricated modules. The first is a thin-film-based micro-grating triboelectric nanogenerator (MG-TENG). The operation principle of MG-TENG relies on the coupling between electrostatic induction and triboelectric effect.[28-32] Consisting of two sets of complementary micron sized electrode gratings on thin-film polymers, the MG-TENG harvests energy by sliding these surfaces.[32] Based on previous research on this technology, a 0.6g MG-TENG with an overall area of 60 cm^2 and a total volume of 0.2 cm^3, achieves an average output power of 3W (50mW/cm^2 or 15W/cm^3) and an overall conversion efficiency of roughly 50%, which is sufficient to power regular electronics like light bulbs.[32] These performance parameters highlight that MG-TENGs are a promising and efficient solution for harvesting energy from mechanical energy in ambient conditions. The second module is a triboelectric nanogenerator (TENG) based on two radially arrayed fine electrodes and can generate periodically changing triboelectric potential that induces alternating currents between electrodes. As presented in previous work, at a rotation rate of 3,000 rpm/min, a TENG with a diameter of 10cm can achieve an output open-circuit voltage (V_{OC}) of around 850V and a short-circuit current (I_{sc}) of around 3mA at a frequency od 3 KHz. Additionally, with a load of 0.8 M, the TENG can provide an average output power of 1.5 W

(19mW/cm^2), and the efficiency to an external load can achieve 24%.[24] The small volume, light weight, low cost, as well as high scalability characteristics make the TENG a suitable solution for mechanical energy harvesting for both small-scale self-powered electronics and potentially in the future larger scale energy generation.

Given the potential of TENGs for low cost energy generation for self-powered applications, it is important to assess their environmental profile and carbon footprint by carrying out a detailed lifecycle assessment (LCA). This will provide an indication as to whether they constitute new environmental challenges or not. A great deal of work has been published on LCA of energy harvesting technologies but to the best of our knowledge, other than the comparative LCA of lead zirconate titanate (PZT) vs. potassium, sodium niobate (KNN), both potential materials for piezoelectric energy harvesters[33], no LCA work currently exists on mechanical energy harvesters such as the TENG. Given the limited environmental information on TENGs, LCA is undertaken within the context of other energy harvesting technologies. LCA involves the evaluation of the complete environmental impact of a material or product from the raw materials extraction phase, through the processing as well as usage phases, and final disposal[34]. It is an important technique adopted to highlight environmental hotspots in the production of consumer goods and their global environmental impact[35]. The use of LCA therefore defines and addresses environmental sustainability issues that are essential for future development and upscaling. Significantly perhaps, it steers us clear of the path that will create a new environmental problem while providing the necessary information with respect to the consequences of material or device substitution.

We live in a world dominated by networked product supply chains, complex production technologies, and nonlinear consumption patterns[36, 37]. It is essential therefore, for consumers, industries and policy makers to have the right information in the course of evaluating the environmental consequences of substitute materials (from extraction, designs, fabrication processes to usage)[33]. To date, a detailed cost estimation and techno-economic evaluation and analysis of TENG modules has not been carried out. Such an evaluation is vital regarding the future of TENG technology due to the urgent need to build a cost-efficient industry that can survive with minimal government interventions.[38] Accordingly, the power conversion efficiencies

and the ensuing financial costs of two TENG module designs were analyzed and compared with existing energy harvesting technologies.

In the light of the above, the rest of the paper is structured as follows. In section 2, a brief description of the fabrication processes of both modules of TENG under consideration is presented. Details of the overall methodological LCA principles and techno-economic framework for comparative cost-benefit analysis with existing energy harvesting technologies is presented in section 3. In Section 4, the key findings from the LCA and techno-economic analysis are discussed leading to the summary and final conclusions in Section 5.

2. Fabrication route of micro-grating triboelectric nanogenerator (MG-TENG)

To manufacture the TENG modules, roll-to-roll (R2R) processing is used. R2R processing is a cheap and fast substrate-based manufacturing processes[39, 40], which can build structures in a continuous manner and has become an important manufacturing technology for a wide range of new environmentally friendly and energy-efficient products. Roller-based R2R lines consist of a series of sequential processing steps which begin by feeding input materials and culminate in winding of the finished material. It is often chosen because it can make a sheet or roll at high volume and relatively low cost, a desired attribute for the concepts discussed in this paper. In addition, it is used globally to fabricate high volume commercial products such as, flexible electronics, chemical separation membranes and multilayer capacitors.[38]

Figure 1 (A-C) shows the architectures of Modules A and B, which were assembled with series connections. Module A[32] was developed using a new type of electricity-generation method that takes advantage of triboelectrification, a universal phenomenon created upon contact between two materials. Based on polymer thin films that have complementary linear electrode arrays, the MG-TENG (Module A) effectively produces electricity that is sufficient for powering regular electronics as the two contacting surfaces slide with respect to each other. The shape-adaptive design of Module A suggests that it may be ideal for harvesting energy from a wide variety of mechanical motions. Given its high electric output power and other significant advantages in terms of weight, volume, cost, scalability and adaptability, Module A is a practically promising approach in harvesting mechanical motions for self-powered electronics.

Module B [24] was developed with a new type of planar-structured, electricity-generation method to convert mechanical energy using the triboelectrification effect. Based on a stator–rotator structure that has arrays of micron sized radial sectors, Module B produces output power sufficient for conventional consumer electronics. It also has the potential to harvest energy from a variety of ambient energy from motions such as air flow, water flow and even body motion. The fabrication of Module B requires a series of finely controlled processes, production of patterns with lasers, and vacuum evaporation to produce Au electrodes, while DC sputter is used to produce Cu electrodes. The high precision of the fabrication processes may result, however in a prohibitively high manufacturing cost.

The main functional differences between Modules A and B lie in their mode of operation, performance efficiency and potential applications. Whereas Module A operates in sliding free standing mode, B operates in a rotating free standing mode. Performance efficiency of A was experimentally determined to be 50% with a resulting power output of 500 W/m^2 and an area of 60 cm^2 (see Table 1). For Module B, the calculated conversion efficiency is 24% (78.95 cm^2), with a corresponding power output is 190 W/m^2 (see Table 1). In terms of their applications, Module B offers more robust and reliable applications regarding energy harvesting from water bodies, wind and body motion at ambient. On the other hand, Module A boasts a higher conversion efficiency in comparison with B, but offers less practical applications compared to TENG B.[24, 32]

(A)

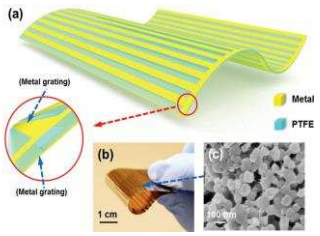

(B)

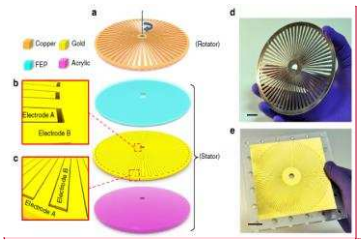

(C)

Commented [T1]: You are still talking about gold. See the above comments from prof Reaney. The section should be re-written to highlight the key difference between the two and the use of gold should be removed

Commented [ir2]: The difference between A and B is not clear enough. This section need rethinking.

Commented [T3]: Gold is still showing in module B

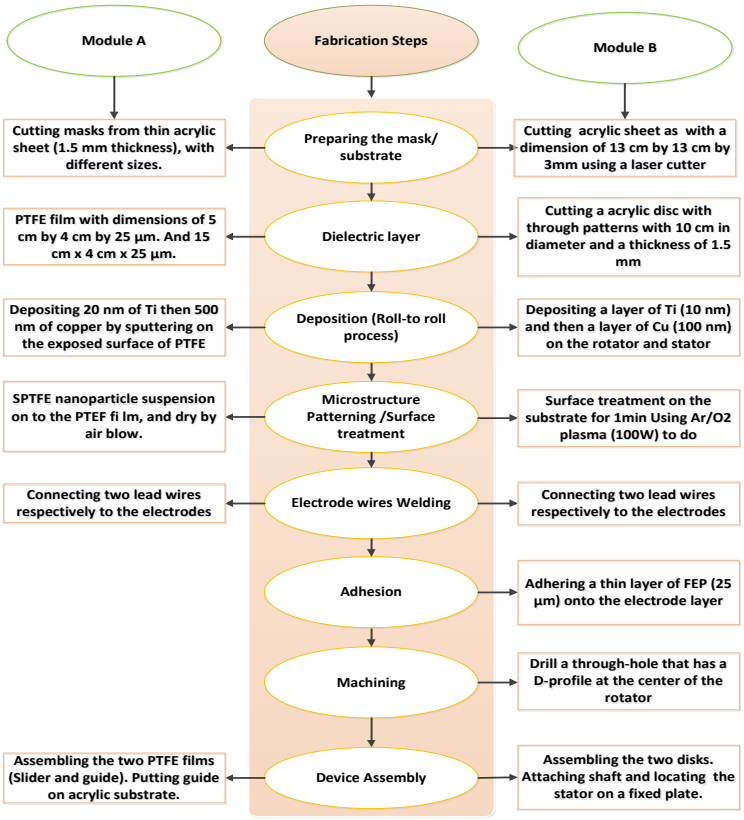

Figure 1: (A) Structural design of the TENG module A; (B) structural design of the TENG module B and (C) fabrication steps for both TENG modules

3. Materials and Methods

In the preceding sections, the phenomenon of triboelectricity as a potential effect for energy harvesting was highlighted. Against this backdrop, detailed environmental profile evaluation and techno-economic analysis of TENG modules are carried out based on the framework schematically illustrated in Figure 2.

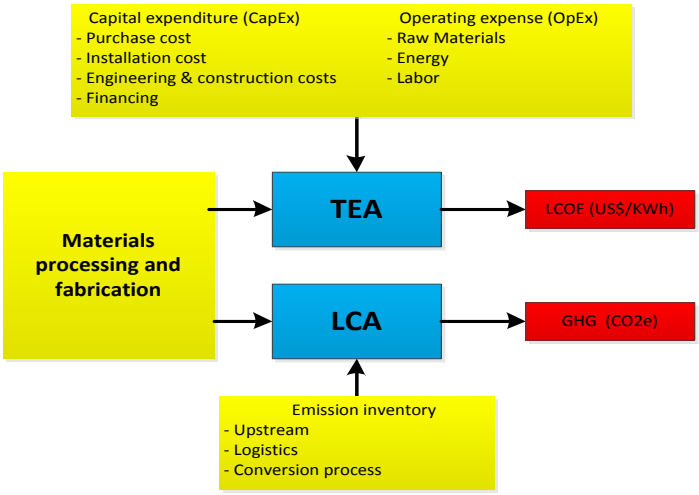

Figure 2: Schematic representation of the overall framework for life cycle assessment (LCA) and techno-economic analysis (TEA) of TENG modules

3.1 Life Cycle Analysis Framework

LCA can be used as a decision-making tool for the systematic tracking of a wide spectrum of environmental impacts across the entire value chain of the development of a product,[41] identifying baskets of interventions for reducing environmental impact without burden shifting.[35, 42] LCA entails the gathering and evaluation of the inputs, outputs, and potential environmental impacts of a product system throughout its lifespan and involves four key steps namely: (i) goal and scope definition, where questions such as what, how and why regarding the LCA work are asked and where the systems boundaries and functional unit are set; (ii) inventory analysis where inputs and outputs data of each process in the life cycle are collated, adding them across the entire system; (iii) evaluation of the environmental effects, detailing LCA results through classification and characterization for comparative analysis; (iv) the interpretation of the inventory and impact assessment of results and the identification of issues that are of significant importance.[34, 43, 44]

The goal of this study is to assess the potential life cycle impacts of two TENG modules (A and B). The overall assessment includes five main steps: i) gaining an understanding of the TENG technology in terms of raw material requirements, production and fabrication processes

of the modules; ii) characterization of the system (i.e. establish systems boundaries, functional unit, modular components, material composition, operational efficiencies etc.); iii) construction of system inventory (e.g. input requirements (physical units), process flow, energy flow, material flow, and reference flow; iv) overall impact assessment and environmental profile evaluations across multiple sustainability metrics; v) performance evaluation and techno-economic analysis. In this work, the functional unit is set as 1 m^2 of the TENG module and all of the inventories generated are converted by aligning them to conform to the functional unit based on the defined systems boundary, as schematically illustrated in Figure 3.

The TENG module is assembled by depositing the components onto the substrate. The manufacturing process consumes energy and produces emissions. After the TENG module is utilized and decommissioned, the waste modules are landfilled in the disposal stage. Disposal mechanism including incineration and waste recycling, are not taken into consideration within the system boundary drawn due to the dearth of data regarding combustion processes or waste recycling for TENG modules. Modular use phase and transportation are also excluded from the system boundary in line with assumptions made in a number of LCA studies for energy harvesting technologies such as photovoltaics.[45-47] Although input-output data can be augmented with process-based data within a hybrid LCA framework[33] to complete the system boundary based on missing data, such an approach is not considered in the current work. The balance of system (BoS) is omitted as part of the overall system boundary to ensure direct like for like comparison with those of other energy harvesting technologies.

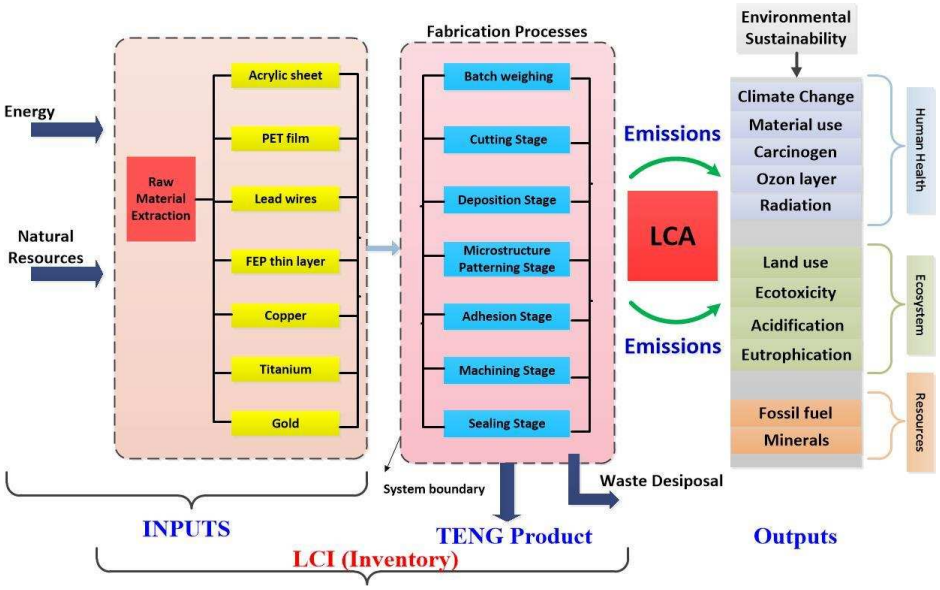

Figure 3: System boundary considered in the LCA, showing the material composition and energy flows associated with the fabrication steps captured within the inventory.

3.1.1 Life cycle inventory

The construction of the life cycle inventory (LCI) is central to any LCA work. Based on the system boundaries described in Figure 3 we classified the LCI of each module into two categories namely material inventory and energy inventory. A material inventory table consists of the mass of raw materials, direct emission during manufacturing, and disposal materials per functional unit of the module. In this analysis, the focus is on two representative solution processed TENG modules. The major differences between the Module A and B are listed in Table 1.

Table 1: Differences between two TENG modules

Module parameters	Module A	Module B
"TENG" Module size	60 cm^2	78.95 cm^2
Distance between TENG unit	1 cm	1 cm
Module efficiency	50 %	24 %
Power output of one piece of module W	3	1.5
Power output of one piece of TENG W/m^2	500	190

The material inventory of 1 m^2 functional unit of Module A is shown in Table 2. The active area ratio and the module efficiency are 90.0% and 50 %, respectively.[32] The masses of the cleaning solvents, PTFE, and acrylic are obtained from the literature [24, 32]. The masses of electrode layer copper and titanium are derived based on the thickness of the corresponding layers, the active area ratio of the module, and the material utilization efficiency. Since the material utilization efficiencies are not reported for TENG modules, we assume that the material utilization efficiencies for laser cutting and sputtering are 30.0% and 75.0% respectively. The mass of direct emission is determined as the mass of the cleaning solvents of ethanol, acetone and deionized water.

The energy inventory of 1 m^2 of the TENG module A is shown in Table 3. As shown, all the operations are performed using electric equipment. Therefore, energy consumption is evaluated by multiplying equipment power by corresponding operating time. We apply the same energy consumption as that evaluated by Espinosa et al [46]. The total electricity consumption for manufacturing 1 m^2 of the TENG module is 1.14 kWh. We translate the electricity consumption in manufacturing the TENG modules to the equivalent primary energy consumption assuming that the electricity applies to the average electricity mix in the US. [48] The end-of-life primary energy consumption accounts for the energy usage involved in landfilling the waste modules.

Table 2: Material inventory of 1 m^2 of the TENG Module A with 90% active area

	Mass (Kg)	Usage
Raw materials		
Substrate patterning		
Acrylic sheet E	1.18E+00	Substrate
Ethanol	1.00E-05	Substrate Cleaning Solvent
Deionized water	1.00E-05	Substrate Cleaning Solvent
Acetone	1.00E-05	Substrate Cleaning Solvent
Grating patterning		
PTFE film E	1.10E-01	3*Layer thickness 25 μm
Ethanol	6.00E-05	Grating Cleaning Solvent
Deionized water	6.00E-05	Grating Cleaning Solvent
Acetone	6.00E-05	Grating Cleaning Solvent
Electrode deposition		
Copper ETH U	2.24E-02	5*Layer thickness 500 nm
Titanium I	4.43E-04	5*Layer thickness 20 nm
Electrode Wires		
Lead ETH U	2.30E-03	Wire diameter 0.01", length 4 m

Direct emission		
Ethanol	7.00E-05	Cleaning Solvent
Acetone	7.00E-05	Cleaning Solvent
Disposal materials	1.32E+00	To landfill

Table 3: Energy consumption for manufacturing 1 m² of the TENG Module (A) with 90% active area

	Power (W)	**Time (S)**	**Electricity (MJ)**
Substrate cutting			
Laser cutter machine	1.50E+03	8.50E+01	1.28E-01
Grating patterning			
Laser cutter machine	1.50E+03	2.55E+02	3.83E-01
Electrode deposition			
Titanium coating/Sputtering	1.50E+03	4.00E+02	6.00E-01
Copper coating/ Sputtering	1.50E+03	2.00E+03	3.00E+00
			Total 1.14 KWh

Tables 4 and 5 summarize the material and energy inventories of 1 m^2 of the Module B, respectively. The mass of Module B is evaluated from the data reported in the literature [24].

Table 4: Material inventory of 1 m² of the TENG Module B with 78% active area

	Mass (Kg)	**Usage**
Raw materials		
Substrate patterning		
Acrylic sheet E	2.27E+00	Substrate
Ethanol	3.00E-05	Substrate Cleaning Solvent
Deionized water	3.00E-05	Substrate Cleaning Solvent
Acetone	3.00E-05	Substrate Cleaning Solvent
Grating patterning		
FEP film E	7.05E-02	Layer thickness 25 μm
Ethanol	3.00E-05	Cleaning Solvent
Deionized water	3.00E-05	Cleaning Solvent
Acetone	3.00E-05	Cleaning Solvent
Adhesive	2.50E-04	Epoxy Resin
Electrode deposition		
Copper	5.374E-03	Layer thickness 200 nm & Layer thickness 100 nm
Titanium	8.86E-05	Layer thickness 10 nm
Electrode Wires		
Lead	2.30E-03	Wire diameter 0.01", length 4 m
Direct emission		

Ethanol	6.00E-05	Cleaning Solvent
Acetone	6.00E-05	Cleaning Solvent
Disposal materials	2.35E+00	To landfill

Table 5: Energy consumption for manufacturing 1 m² of the Module B with 78% active area

	Power (W)	Time (S)	Electricity (MJ)
Substrate cutting			
Laser cutter machine	1.50E+03	3.50E+03	5.25E+00
Grating patterning			
Laser cutter machine	1.50E+03	2.00E+01	3.00E-02
Drilling	2.20E+03	2.00E+01	4.40E-02
Air/O_2 plasma	1.00E+02	6.00E+01	6.00E-03
Electrode deposition			
Titanium coating	1.50E+03	5.00E+02	7.50E-01
Copper coating	1.50E+03	5.00E+03	7.5E+00
Total			1.36E+01
			3.78 KWh

3.1.2 Life cycle impact assessment modelling

The overall impact assessment based on the LCI above was performed following the guidelines provided in the International Organization for Standardization (ISO) 14040[49] and 14044[50]. This allows for the appropriate data management of life cycle inventory and assessment of environmental impacts stemming from each of the materials used for the fabrication of the TENG modules over their life cycle. Each entry life cycle inventory developed for this work was matched with an appropriate unit process in conformity with the functional unit. Using life cycle inventories, the environmental impacts were calculated as follows[33, 51]:

$$B_j = \sum_{i=1}^{I} b_{j,i} \times x_i \qquad j = 1,2,\dots\dots\dots,J \tag{1}$$

$$E_k = \sum_{j=1}^{J} e_{k,j} \times B_j \qquad k = 1,2,\dots\dots\dots,K \tag{2}$$

Where:

$b_{j,i}$ is the environmental burden j per unit activity i, with burdens constituting raw materials and energy consumed within the system and emissions to air, land and water. These parameters are obtained from LCA software and databases such as SimaPro and Ecoinvent[52]. x_i is the mass or

energy flow associated with unit activity i. $e_{k,j}$ is the relative contribution of the total burden B_j to impact E_k as defined by the CML 2001 method.[53]

The overall focus of the current work is on global warming potential (GWP). However, the need to consider multiple sustainability metrics when analyzing the environmental profile of a product or process was demonstrated by Ibn-Mohammed et al.[33] This will, for environmental trade-off analysis, ensure that greenhouse gas (GHG) emissions are not minimized at the expense of other indicators including human toxicity, acidification, eutrophication, material use, fossil fuel and ozone layer depletion.

3.2 Techno economic evaluation of TENG Modules

3.2.1 Module cost estimation

To assess the cost of fabricating the modules, we assumed the production capacity of both routes to be 100 MW per year. As shown in Figure 4, the module cost consisted of the capital, materials and overhead cost. The capital cost is calculated based on depreciation of capital investment (CI). Given that the complete process of Module A was based on the fabrication steps in Figure 1, the CI was taken to be $7 million for a production capacity of 100 MW (see Tables S1 and S2 in the supporting information (SI) document). Module B has an efficiency of 24% which is lower than of Module A (50%), as such, the capital investment for Module B (CI Module B) for a 100 MW capacity per year was estimated to be $14 million per year (see Tables S1, S3). Details of how the cost estimates were made are presented in Table S2 and Table S3 of the Supporting Information.

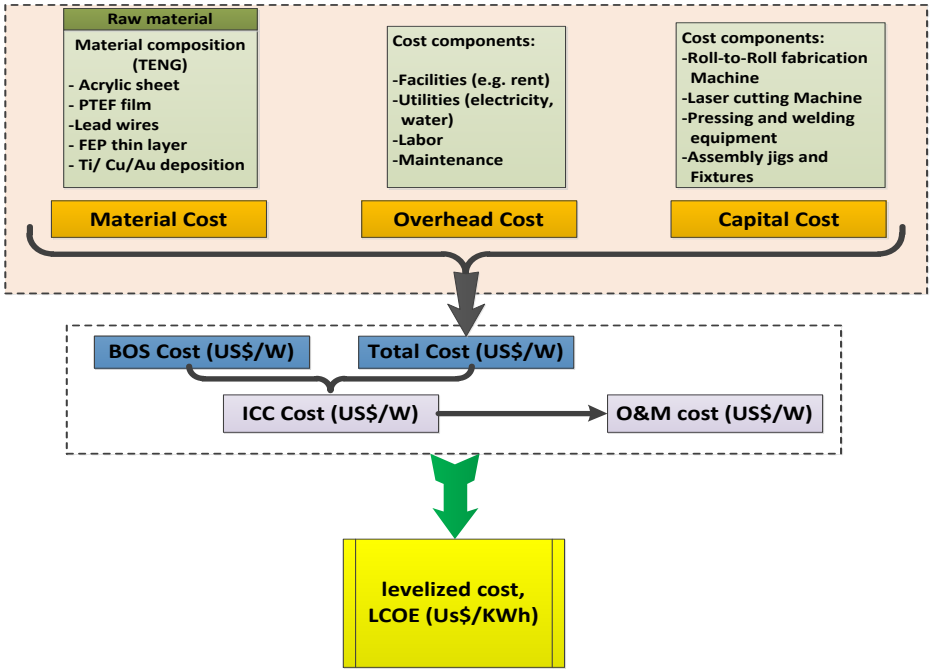

Figure 4: Cost parameters considered for the techno-economic analysis of TENG modules detailing the relevant materials, overhead costs, capital costs and levelized cost.

The depreciation of the facility resulted in a decrease of capital investment from year to year according to Equation (3):[54]

$$(CI)_n = CI \times \beta^n \qquad (3)$$

where n is the number of years after construction and β is the depreciation ratio, which is assumed to be 0.5 based on information from the nascent industry of TENG developers. Depreciation of an investment should cease when $\beta^n < 0.1$. After four years, there was no further depreciation of the investment because $(0.5)^4 = 0.063$. The capital costs of Module A and B were based on the ratio of capital investment to power output, which changed from \$US0.07/W to \$US 0.004375/W and from US\$ 0.14/W to \$US 0.00875/W, respectively, during the first five years (see Table S4 and Table S5 in the supplementary information for details). The module cost was calculated by summing the capital amortization, materials, and overhead costs. The capital amortization costs

for Module A and B were taken to be $US 0.016/W and $US 0.032/W, respectively, based on the annual worth of CI (1.6 million USD for Module A and 3.2 million USD for Module B); they were equated to:

$$\frac{i \times (1+i)^n \times CI}{(1+i)^{n-1}} \quad (4)$$

where i is annual interest and n is 5-year equipment lifetime. Annual interest of 5% was assumed for 2020, based on current low global interest rates. The costs of materials for Module A and B were estimated to be US$/0.617 W and US$/2.56 W, respectively, based on the ratio of investment in materials to power output with material usage of 80%. The overhead costs consist of labor, the renting facilities and utilities. The labor cost of US$0.0304/W was estimated based on the flexible electronics industry average (see Table S7, supporting information for details). Based on similar industry of DSCs and thin-film, silicon solar cell manufacturing lines, the rents for Module A and B were estimated to be US$0.00792/W and US$0.022/W, respectively. The utilities cost for Module A and B were estimated to be US$0.00792 /W and US$0.022/W, respectively. After adding 1% of the capital costs for maintenance fees ($US 0.0016 million /year and US$0.0016 million/year for Module A and B (Table S8, SI), the overhead costs of Module A and B were calculated to be US$ 0.04784/W and US$0.075/W, respectively (Table S8, SI).

The resultant module costs calculated based on our assumptions were US$0.68084/ W and US$2.667/ W for Module A and B, respectively (Table S9, supplementary information). These were the baseline values used in the sensitivity analysis (Section 4.5.2). Estimation of the levelized cost of electricity were based on the total cost of a solar cell system, including the costs of the module, balance of systems (BOS), land, support structures, wiring, power conditioning and installation, [54] and summed according to Equation (5): [55, 56]

$$LCOE = \frac{ICC \times 1000CRF}{CF \times 8760} + O\&M \quad (5)$$

where ICC is the Installed Capacity Cost ($/W DC) = BOS cost + module cost; CRF is the Capital Recovery Factor, expressed as:

$$CRF = \frac{i(1+i)^n}{(1+i)^n - 1} \quad (6)$$

where $\boldsymbol{i}$ is the discount rate and $\boldsymbol{n}$ is the useful lifetime (i.e. lifetime of system), CF is the alternating Current Capacity Factor, calculated as 0.8 × renewable energy source e.g. wind energy/8760 hours. This factor is reduced by 37% due to losses during switch from direct current to alternating current. O&M is the operation and maintenance cost expressed in $/kWh.

The following assumptions were made. BOS was $US 75/m^2 based on based on the projected long term goal silicon based solar cells in 2020[57]. BOS costs at an efficiency of 50% and 40% for module A is $US 0.15 /W and US$0.1875/W respectively. For module B, with an efficiency of 24% and 20%, the corresponding costs is US$0.394/W and US$ 0.474/W, respectively. By using BOS cost = 75 US$ × m^2/output; O&M = $0.001/kWh; i = 5%, and n = 20 (no tax credits and no accelerated depreciation), from these values, CRF (i = 5%, n = 15) = 0.1. To derive the energy produced per year due to 1 W of installed TENGs a CF of 37% was assumed.

Commented [T4]: Not clear

4. Results and discussion

4.1 Primary energy consumption and carbon footprint

Primary energy demand and by extension the carbon footprint due to the fabrication of both TENG modules is the focus of the current LCA work with a view to identifying hotspots in the entire supply chain of the modules. Based on the constructed LCIs in Tables 2 to 5, the primary energy consumption and their corresponding carbon footprint distributions for TENG modules A and B are evaluated and depicted in Figures 5 and 6, respectively. As indicated in Figure 5, about 90% primary energy consumed in both modules is attributed to raw materials requirements. A disaggregation of the materials embodied energy highlights the key variances between the TENG modules. For instance, in the Module A, acrylic (78.18%) and polytetrafluoroethylene, PTFE (20.48%) are the major contributors to the materials embodied energy. Similarly, the distribution of embodied materials energy is dominated by acrylic, fluorinated ethylene propylene (FEP film), and copper with each contributing 96.88%, 2.87% and 0.25% respectively. As indicated in Table 2 and Table 4, the quantity of acrylic in the materials composition of both modules A and B are 1.18kg and 2.27kg, explaining their dominance in the total mass of the modules (78.18% for the module A and 96.88% for the module B).

In terms of electrical energy consumed (also expressed in MJ/m^2 to conform to the unit of materials embodied energy), electrode deposition of copper coating/sputtering consumed the

largest amount of energy (~73%) due to the length of time associated with carrying out such activity during fabrication of Module A. Electrical energy consumed by sputtering titanium coating deposition and laser cutting machine constitute roughly 15% and 13%, respectively. Overall, electrode sputtering consumes ~85% of the electrical energy for the fabrication of Module A. Adoption of alternative deposition techniques for copper and titanium coating would go a long way in minimizing the overall electrical energy consumption. As for Module B, the increased number of operations involved in its fabrication resulted in higher electrical energy consumption compared to Module A. As with Module A, sputtering of titanium and copper consumes ~62% of the electrical energy with laser machining and associated drilling activities consuming 38%. Sputtering as a means of depositing thin film of the metals in the modules guarantees high quality but comes at high cost.[58] Overall, module B consumes more electrical energy during fabrication compared to module A.

Figure 6 shows the distribution of carbon footprint from which the major contributors of the substrate, the copper electrode, sputtering and laser cutting can be established. The distribution of primary energy consumption during fabrication indicates similar patterns to the carbon footprint because different fabricating operations consume only electricity and their conversion to carbon dioxide equivalent (CO_2-eq) are based on the appropriate characterization factors in the evaluation process. Not only the distributions of primary energy consumption and the carbon footprint exhibit similar pattern, but those of other impact categories remain identical, provided the steps involved in the fabrication remains constant. A resemblance can be found between the distributions of the material embedded primary energy consumption and the carbon footprint, which suggest similar strategies for optimizing both modules for improved environmental performance could be adopted.

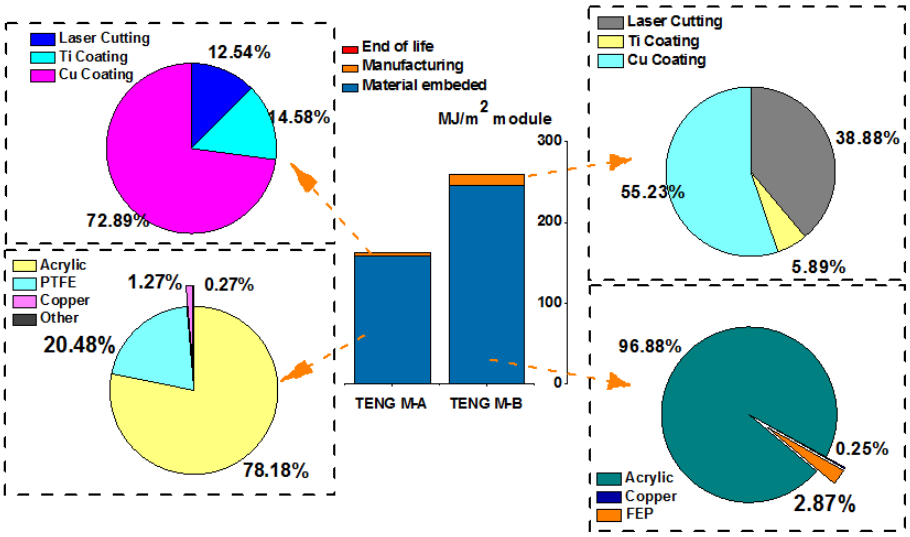

Figure 5: Distributions of the primary energy consumption for fabricating two TENG modules.

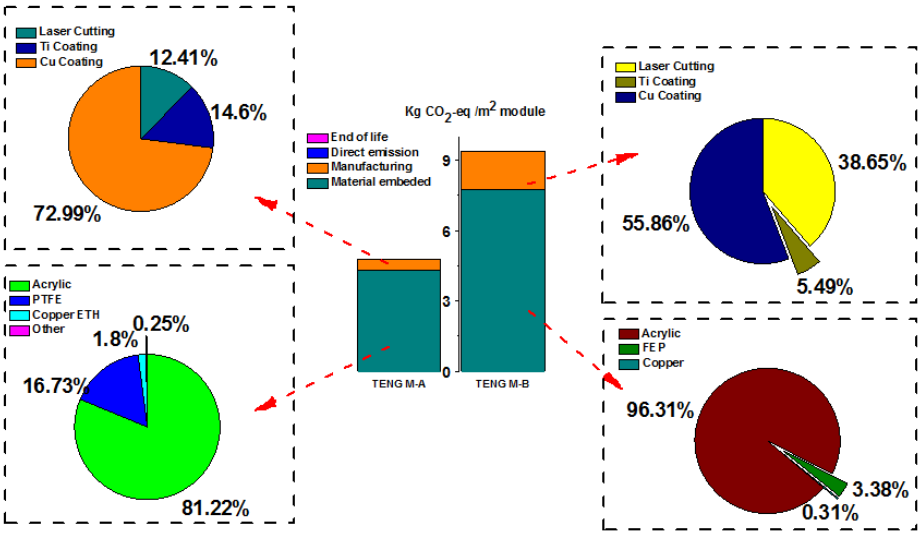

Figure 6: Distributions of the carbon footprint of TENG Module A and B.

4.2 Environmental profile assessment of contributing components of TENG Module A and B across multiple indicators

Figures 7 and 8 show the environmental profiles of 1 m^2 of the TENG module A and 1 m^2 of the TENG module B, respectively. All 11 environmental impact metrics are normalized to 100% with the view that the sum of the impact of each of the contributing processes or materials is 100%. As indicated in Figure 7, the acrylic is the most significant contributor for carcinogens (82%), respiratory organics (85%), respiratory inorganics (73%), climate change (74%), acidification/eutrophication (76%), fossil fuels (81%), and ecotoxicity (33%). Although the intensity of materials embodied energy and CO_2-eq of copper, lead and titanium are numerically higher than that of acrylic, but given that the quantity of acrylic in the materials composition is highest, its overall impact across the aforementioned impact categories outweighs other materials. Sputtering due to electrical energy consumption also has great influence on radiation (96%), ozone layer (83%), and land use (83%). The use of acrylic however, offers an advantage in the fabrication of the modules. For instance, acrylic has very good structural properties such as lightweight, ease of fabrication, impact resistant and ability to withstand poor weather conditions. Its high strength and durability is also an advantage. Furthermore, acrylic sheets are fabricated using fabrication processes in facilities that are certified by ISO-14001. More importantly, the scenario of their end of life is environmentally viable given their recyclability and reuse potential. Additionally, compared to other plastics that produce toxic gases that are harmful to humans and the environment during combustion processes, acrylic does not pose such threats due to its stability during exposure to ultraviolet radiation.

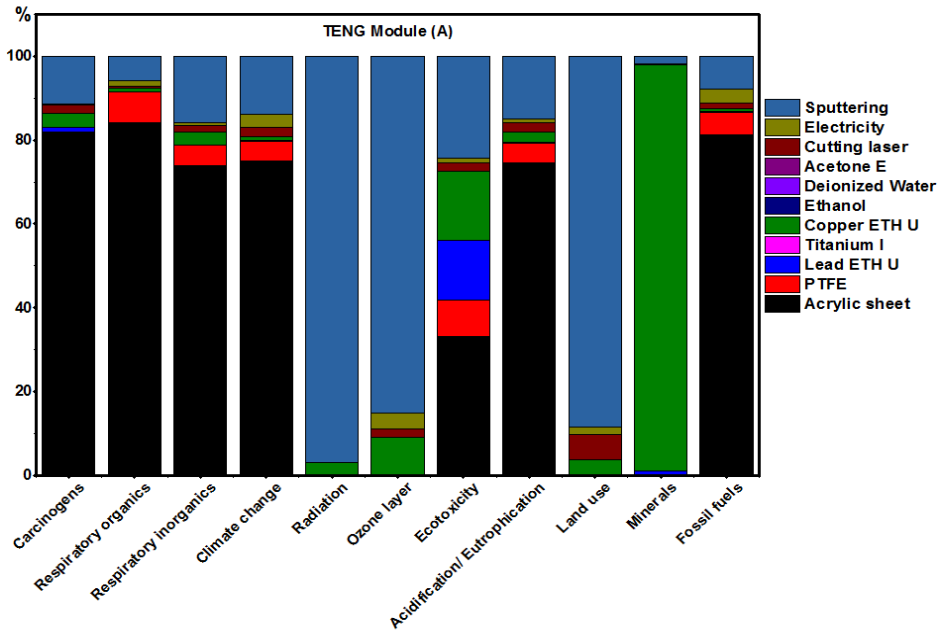

Figure 7: Environmental profile of 1 m^2 of the TENG module A.

As shown in Figure 8, for the TENG module B, the presence of acrylic as in module A, also constitutes the major influence across a number of indicators. For instance, the use of acrylic is the most significant contributor for carcinogens (83.1%), respiratory organics (~92%), respiratory inorganics (80.8%), climate change (81%), acidification/eutrophication (79.5%) and fossil fuels (88 %). The reason for this is similar to that of module A (i.e. the quantity of acrylic used dominates those of other materials in the architecture). Sputtering due to electrical energy consumption also has great influence on radiation (88%), ozone layer (70%), and land use (70%).

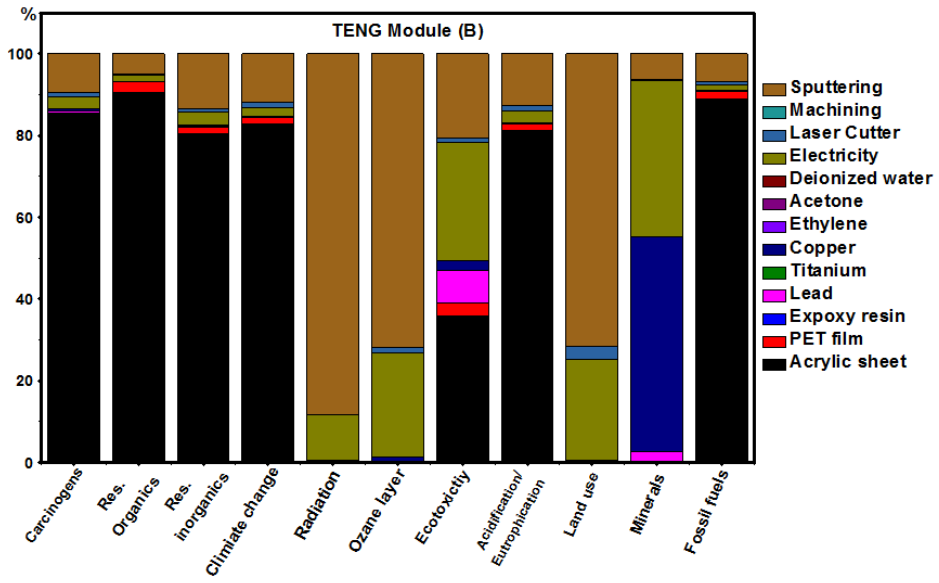

Figure 8: Environmental profile of 1 m^2 of the Module B

Comparative life cycle impact assessment results between the two TENG modules is depicted in Figures 9 through 11. Module A is used as the standard for normalization. In Figure 9, Module A performs better environmentally than module B except in one impact category, minerals. This is attributed to the higher quantities and triple layer thickness of polytetrafluoroethylene (PTFE) used in module A compared to single layer thickness of fluorinated ethylene propylene (FEP film E) used in module B. PTFE is generated through polymerization of tetrafluoroethylene using free radicals, hence the high mineral resource requirements. The uniformity of its materials structure (i.e. PTFE), its excellent chemical, electrical and physical properties, its tightly controlled thickness as well as its inherent capabilities to serve as a semi-permeable membrane renders it applicable for TENG and biomedical applications[59]. On the other hand, the compatibility of FEP with various chemicals, reliable electrical properties, mechanical toughness and broad thermal range makes it suitable for TENG applications[60].

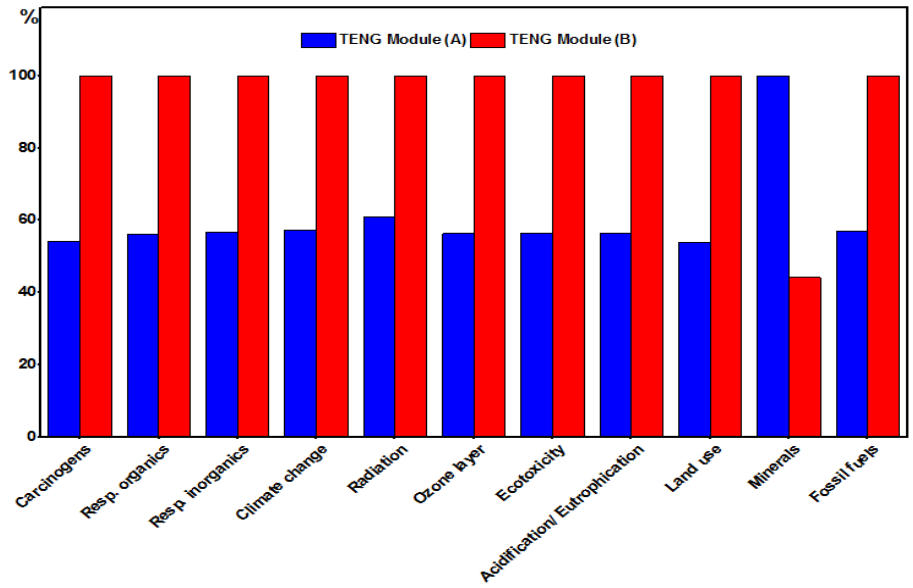

Figure 9: Comparison per damage category, by summation of individual impacts, the higher impact set equal to 100, Eco indicator 99 Europe E/E methodology

Figure 10 displays proportions between impacts of the two types of TENG modules with respect to eco-indicator 99 under human health, resources and ecosystem quality. As shown, Module B caused more damage compared to Module A. Single score comparison by impact category based on Eco indicator 99 is depicted in Figure 11, where the environmental impact of module B also surpasses that of module A. For further comparative results of the environmental profile of TENG modules, we refer readers to the SI.

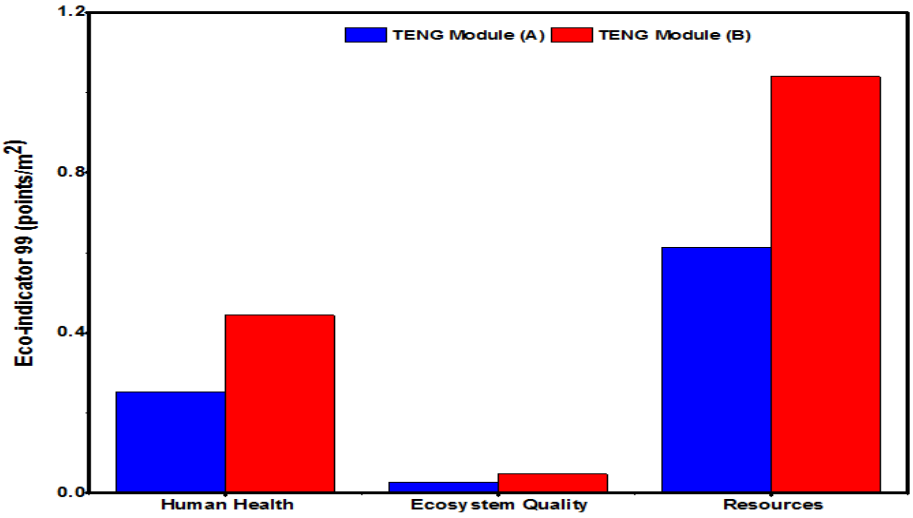

Figure 10: Endpoint comparison after weighing, Eco indicator 99 Europe E/E methodology

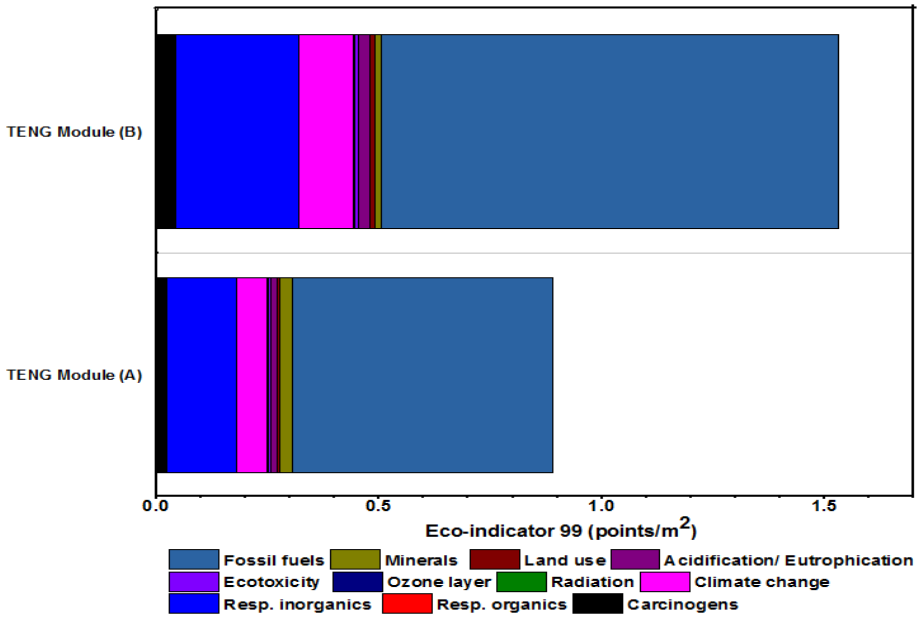

Figure 11: Single score comparison by impact category, Eco indicator 99 Europe E/E methodology

4.3 Comparison with existing energy harvesting technologies

4.3.1 Eco-indicator

Eco-indicator 99 results across ecosystem quality, resources and human health for eight variants of energy harvesting technologies, notably PV modules, were compared with the TENG modules as depicted in Figure 12. In all three damage categories, both modules achieved the lowest points and are one order of magnitude lower than those of c-Si, a-Si, ribbon-Si, CdTe, CIS, OPV TiO_2 and ZnO PV modules. This clearly demonstrates the overall environmental edge of the TENG modules when compared to PV technologies. Therefore, a more environmentally sustainable energy harvesting technology could potentially be developed based on TENG modules, although this may require switching to greener substrates and reducing the consumption of organic solvents as well as the use of efficient fabrication processes.

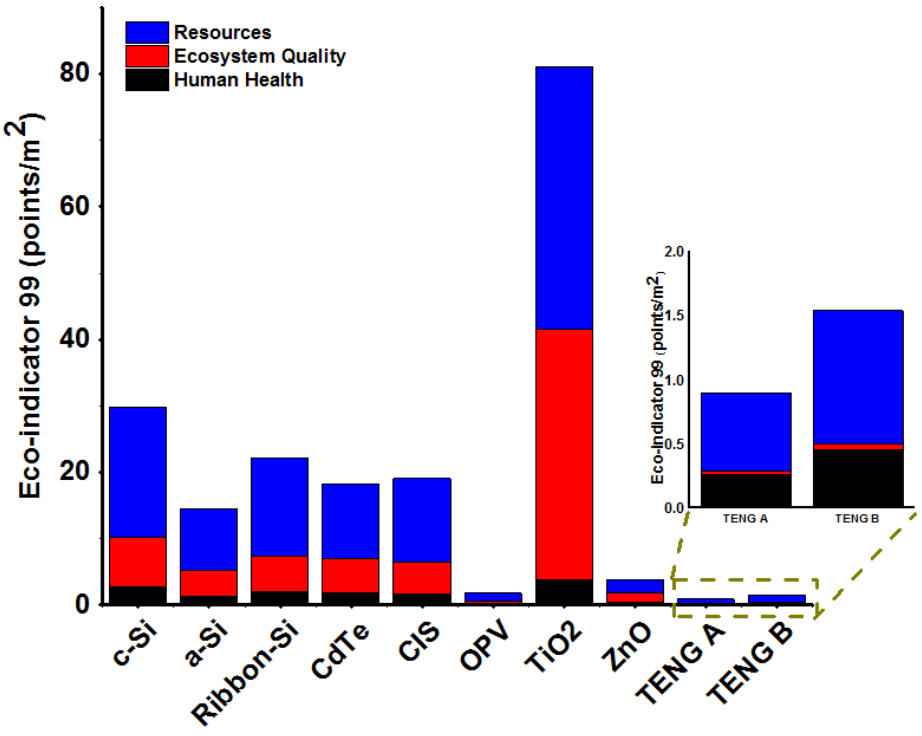

Figure 12: Eco-indicator 99 results for 1 m^2 of each module. The data for c-Si, a-Si, ribbon-Si, CdTe, and CIS are extracted from the study of Laleman et al.[61] The data for OPV are extracted from the study of Espinosa et al[46]. The data for TiO_2 perovskite module and ZnO perovskite module were based on the work of Gong et al.[62]

4.3.2 Energy payback period

In this section, the energy payback periods (EPBP) of Modules A and B are compared with existing PV technologies (i.e. silicon technologies, thin-film technologies, organic solar cells and perovskite solar cells). The EPBP is given by:

$$\text{EPBP} = \frac{\text{Embodied energy (kWh/m}^2\text{)}}{\text{Energy output (kWh/m}^2\text{/year)}} \quad (7)$$

The result of the comparison is shown in Figure 13. As shown, Module A has a shorter nominal EPBP than the other technologies at 0.05 years. Module B also has a shorter EPBP compared to traditional PV technologies but higher than those of organic and perovskite solar cells. The reason for TENGs outperforming silicon and CdTe based PV cells is because their fabrication does not have high energy intensity requirements associated with silicon or rare element purification and processing that causes higher environmental impact[62]. This is largely due to the efficient fabrication routes based on R2R processing. It is important to note that the EPBP of Module B is higher than those of OPV and perovskite solar cells, attributed to its lower energy output relative to the aforementioned technologies. Nevertheless, in the future, by leveraging on optimal and efficient processing technologies, the EPBP of TENGs can be further reduced significantly. Overall, the favorable environmental profile and EPBP of the TENG modules compared to the traditional energy harvesting technologies suggest that in the future, they can challenge the existing technologies, whilst contributing immensely towards addressing global energy problems.

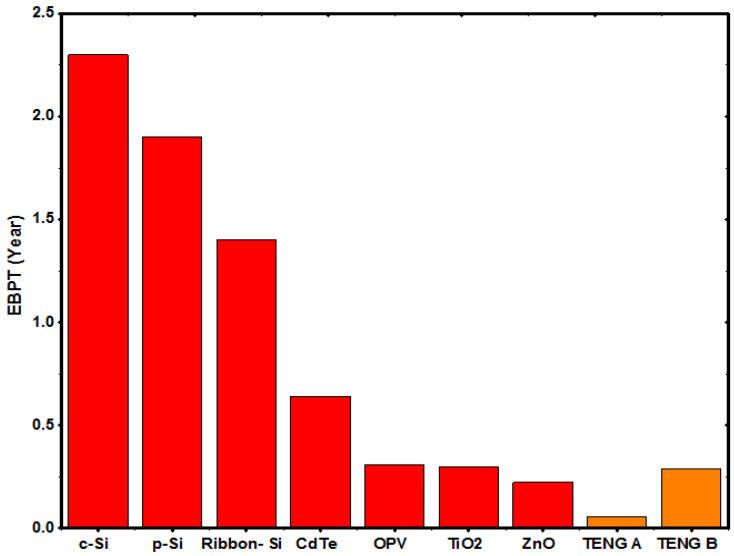

Figure 13: Comparison of energy payback time for 7 PV modules with TENG modules. The data for the energy payback period of all the PV modules were based on the work of Gong et al.[62]

4.3.3 CO_2 emission factor

The CO_2 emissions factor (CEF) is given by:

$$\text{CEF} = \frac{\text{Carbon footprint (kg } CO_2\text{eq)}}{\text{Energy output across the lifespan (kWh)}} \qquad (8)$$

To apply Equation 8, the lifespan of the TENG system under consideration must be established. Lifespan of other existing PV technologies are already well-established. Likewise, assumptions have been made about the lifespan of perovskite solar cells. Given that TENGs are still in their infancy, no exact value in terms of lifespan has been reported for them. Figure 14 shows the comparison of CO_2 emission factors for existing energy harvesting technologies to TENG modules. As indicated, CO_2 emission factors for both types of modules are similar to OPV and perovskite solar cells (although Module A shows a slightly lower CEF). This suggests that the associated cost of CO_2 is currently high due to their shorter lifespan (assumed to be 2 years). In the future, it is expected that the lifespan of TENGs will increase considerably due to material optimization, thereby lowering their CEF.

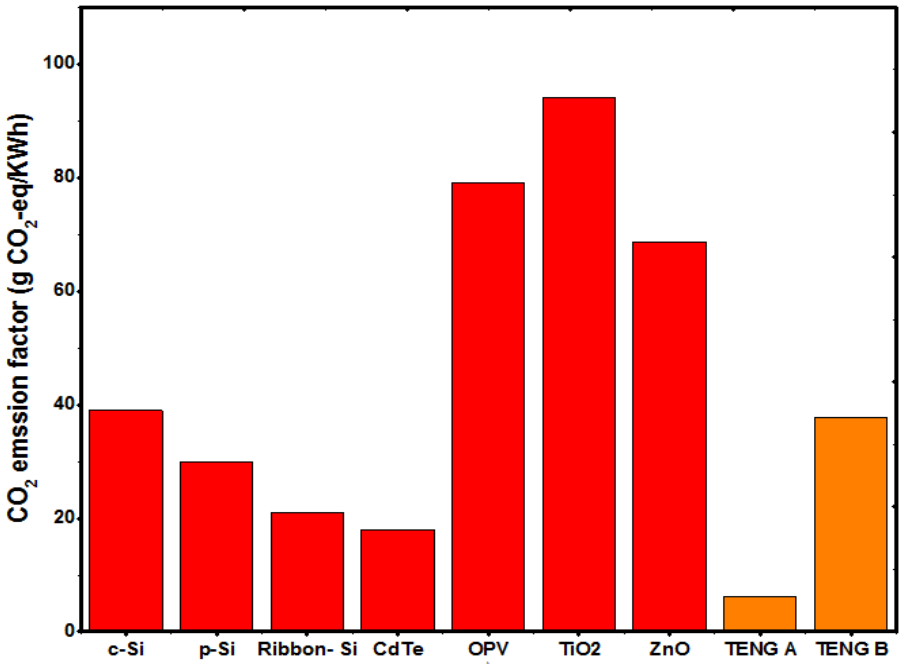

Figure 14: CO_2 emission factor for selected PV modules and 2 TENG modules A and B. The data for the CO_2 emissions factor of all the PV modules were based on the work of Gong et al.[62]

4.4 Sensitivity analysis

The probability distributions of the two forecasts for the TENG modules are shown in Figure 15 and 16. Both distributions demonstrate a wide range, with the highest bars representing the values of the highest probabilities. The asymmetric profile of both distributions results from the nonlinear relationship between the input parameters and the sustainability indicators. The simulation results are shown in Figure 15 and 16. The single cores in both cases are comparatively robust when the key specifications of the module are subject to uncertainty. The low single core points for the entire 95% confidence regions demonstrate that TENGs are already environmentally competitive.

A sensitivity analysis was also conducted to estimate how the environmental performance of Module A and B altered if the consumption of material and energy during manufacture is varied, given the dominating influence of some input parameters across all the considered impact categories. For each parameter, two scenarios were modeled and then compared with the baseline, i.e., a 10% decrease and 10% increase of the total consumption. As shown in Tables 7 and 8, the

variation of acrylic consumption influences the Resp.organics impact most. For instance, a ±10 % variation of cement consumption would lead to a ±8.4 % and ±9.1 % change of the Resp.organics impact in Modules and B respectively. As expected, the minerals impact is most sensitive to the variation of electrode deposition consumption, and a 10% decrease of electrode deposition would lead to a ±9.7% and ±4.8% corresponding drop of this indicator for Module A and B. The fluctuation of manufacturing during the construction and operation would lead to the largest value change of radiation and about ±9.6% and ±10% variation occurs for Modules A and B, respectively, if the former changes by 10 %.

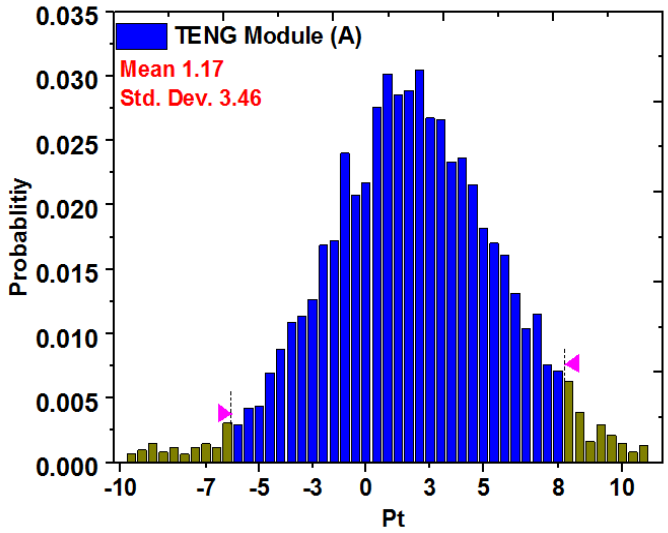

Figure 15: Probability distributions for the single core impact category of Module A.

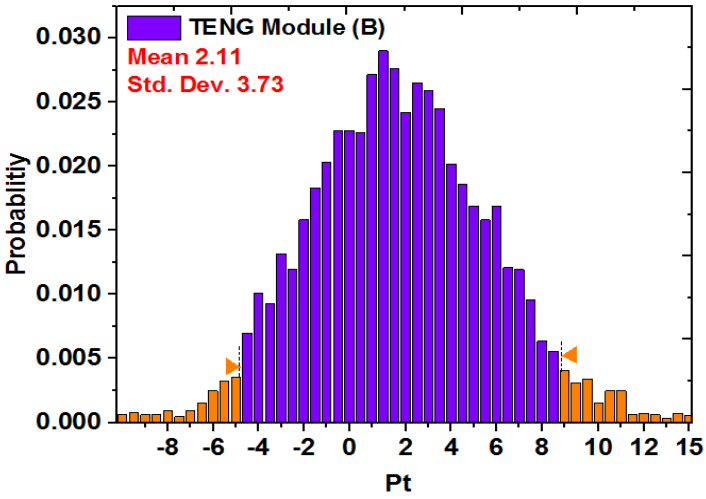

Figure 16: Probability distributions for the single core impact category of Module B.

Table 8 Sensitivity analysis results for the Module A

Input	Variation (%)	Carcinogens	Resp.organics	Resp.inorganics	Climate change	Radiation	Ozone layer	Ecotoxicity	Acidification/ Eutrophication	Land use	Minerals	Fossil fuels
Acrylic	-10	+8.2	+8.4	+7.4	+7.5	0.0	0.0	+3.3	+7.5	0.0	0.0	+8.1
	+10	-8.2	-8.4	-7.4	-7.5	0.0	0.0	-3.3	-7.5	0.0	0.0	-8.1
PTFE	-10	0.0	+0.7	+0.5	+0.5	0.0	0.0	+0.9	+0.5	0.0	0.0	+0.5
	+10	0.0	-0.7	-0.5	-0.5	0.0	0.0	-0.9	-0.5	0.0	0.0	-0.5
Electrode deposition	-10	+0.3	+0.1	+0.3	+0.1	+0.3	+0.9	+1.6	+0.2	+0.4	+9.7	+0.1
	+10	-0.3	-0.1	-0.3	-0.1	-0.3	-0.9	-1.6	-0.2	-0.4	-9.7	-0.1
Manufacturing	-10	+1.4	+0.8	+1.8	+1.9	+9.7	+9.1	+2.8	+1.8	+9.6	+0.2	+1.3
	+10	-1.4	-0.8	-1.8	-1.9	-9.7	-9.1	-2.8	-1.8	-9.6	-0.2	-1.3

Table 7 Sensitivity analysis results for the Module B

Input	Variation (%)	Carcinogens	Resp.organics	Resp.inorganics	Climate change	Radiation	Ozone layer	Ecotoxicity	Acidification/Eutrophication	Land use	Minerals	Fossil fuels
Acrylic	-10	+4.6	+1.1	+1.6	+2.2	0.0	0.0	+0.43	+1.7	0.0	+0.03	+8.9
	+10	-4.6	-1.1	-1.6	-2.2	0.0	0.0	-0.43	-1.7	0.0	-0.03	-8.9
Gold	-10	4.65	+8.8	+8.1	+7.3	+1.6	+9.2	+8.8	+8	+9.3	0.0	+7.1
	+10	-4.65	-8.8	-8.1	-7.3	-1.6	-9.2	-8.8	-8	-9.3	0.0	-7.1
Electrode deposition	-10	0.0	0.0	0.0	0.0	0.0	+0.1	0.2	0.0	0.0	+4.8	0.0
	+10	0.0	0.0	0.0	0.0	0.0	-0.1	-0.2	0.0	0.0	-4.8	0.0
Manufacturing	-10	+1.4	+0.7	+1.7	+1.5	+10.0	+9.9	+5.1	+1.7	+10	+4.9	+0.9
	+10	-1.4	-0.7	-1.7	-1.5	-10.0	-9.9	-5.1	-1.7	-10	-4.9	-0.9

4.5 Techno- economic analysis

4.5.1 Estimation of Costs of TENG Modules

Figure 17 shows the cost of Module A and B in the 1st and 5th year and amortization capital cost over 5 years. The module cost can be divided by the materials, overhead, and capital cost. The capital costs for Module A and B were calculated based on the capital costs of TENGs fabricated using Table S2 and S3, respectively. The cost of materials was estimated based on the amount used. The overhead cost was estimated based on reasonable assumptions. The details of the calculation are shown in the Methods section and Supporting Information. The relatively high module cost in the first year was due to the high depreciation rate (50%) of capital investment. The calculated capital costs in the first year were 0.07 and 0.14 US$/W for Module A and B, respectively. The initial capital cost of Module A was lower because the capital investment associated with use of large efficiency was higher than that in Module B. However, the capital cost rapidly decreased because of depreciation, the result being a monotonic decrease of the total module cost during the first 5 years (Table S4 and S5). After that time, the contribution of capital cost to total cost lowered, so that, the module cost was determined mainly by overhead and materials costs. Figure 19 presents the distribution of the materials cost for TENG production routes. DSM layers represent device structural materials, D/EM represents electrode dielectric materials and LW for electrode wire. Other materials costs in Figure 17 include the expense on

Commented [ir5]: what are these?

Ti/CU deposition. The total calculated cost of materials for Module A 0.617 US$/W was lower than the cost for Module B 2.56 US$/W (Table S6). The higher cost of materials for Module B was because both output power and efficiency are higher in Module A compared with B.

This result suggests that high efficiency of module can reduce the cost of materials due to enhancement in utilization of materials. The overhead costs of Module A and Module B (shown in Table S7 and S8) were estimated at US$0.04784 /W and US$0.075 /W based on the report of thin film silicon solar cells production. Hence, the conclusion could be drawn that the cost of Module B produced by Module B and that of Module A produced by Module A are almost the same. To compare the module cost with other energy harvesting technologies and calculate the electricity generating cost, the amortization module cost was also calculated by amortizing total capital cost by working lifetime of equipment. As shown in Figure 18, the amortization module costs were calculated as US$ 0.68084 for Module A and US$ 2.667 for Module B (Table S9). These two amortization module costs are used to follow sensitivity analysis and estimate the Levelized cost of electricity which is usually considered as the cost associated with generation.

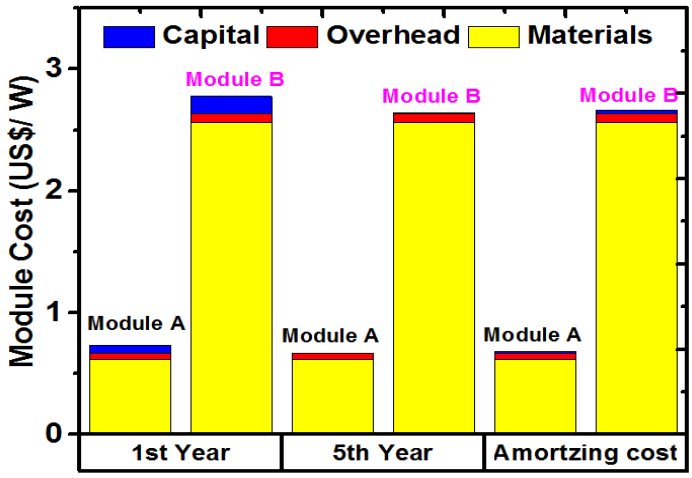

Figure 17 Calculated modules costs of TENGs for first year, fifth year and amortizing over 5 years with taking depreciation and amortizing capital cost into consideration. The depreciation rate was 50% per year and the capital cost was assumed to remain constant after the five-year period.

The module costs of Module A and Module B in the 1st year and 5th year, as well as amortization capital cost over 5 years is demonstrated in Figure 17. In addition, the cost is divided

into material, overhead and capital. The capital costs of Module A and B are based on the capital costs resulting from the fabrication of TENGs, as shown in Table S2 and Table S3, respectively. The material costs are based on the materials used during the fabrication processes. The overhead costs are based on reasonable assumptions. The calculation details can be found in the Methods Section and Supporting Information Section. As the figure indicates, the module cost in the 1st year is relatively high, resulting from the high depreciation rate of 50% in capital investment. The capital costs for Module A and B in the first year were 0.07 and 0.14 US$/W, respectively. Because Module A has a larger efficiency than Module B, its initial capital cost was lower. However, as a result of depreciation, the capital cost decreased monotonically with the module cost in the first 5 years, Table S4 and S5. The total contributions of capital costs lowered after this period, with module costs determined mainly by overheads and material costs.

Commented [ir6]: What are the assumptions

The distribution of the material costs for TENG production is shown in Figure 18 which uses the same nomenclature as Figure 17. As demonstrated in Table S6, the total material cost for Module A is 0.617 US$/W, lower than that of Module B (2.56 US$/W). This is because Module B has a lower output power and efficiency than Module A. Those observations demonstrate that a higher efficiency module can enhance the utilization of materials, and that the total cost of materials decreases accordingly.

Based on thin film silicon solar cell production, Module A and Module B will have total overhead costs of US$0.04784/ W and US$0.075/W, respectively. Therefore, the total production costs of Module A and B are similar. To compare costs between different energy harvesting technologies, and to calculate the costs for electricity generating and amortization, module costs were also calculated by amortizing total capital cost by lifetime of the equipment. The results show that Module A's amortization module cost is US$ 0.68084 whereas Module B's is US$2.667, as shown in Figure 18. These results will be used in sensitivity analysis and estimation of leveled cost of electricity to obtain an estimate the cost of electricity generation.

Commented [ir7]: needs a reference

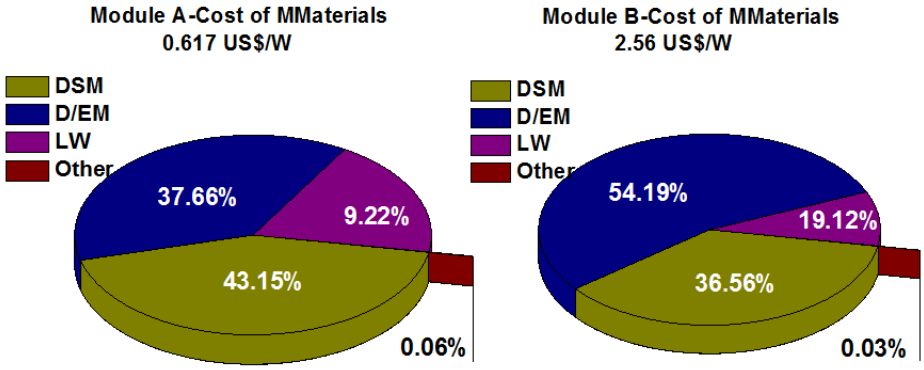

Figure 18: Cost of materials distribution for Module A (left) and Module B (right). The values of materials cost are assumed by the real amount of material used in both structure and wholesale price. The 80% materials usage ratio has been considered.

4.5.2 Sensitivity analysis of Module Cost

It is noteworthy that these cost estimates were based on assumptions about the two kinds of TENG structures. However, the assumed parameters may vary when TENGs are commercialized. Hence, we performed further sensitivity analyses to consider the effect of TENG on module costs. The module costs increased exponentially as their module efficiency decreased (Figure 19). The solid line corresponds to the efficiency of present research status. The efficiency of Module A was assumed to be 20-50% based on a current device efficiency of 40-50%. The corresponding estimated module cost was 0.8308 -0.86834 US$/W. And 15-24% based on a current device efficiency of 20-24% for Module B. The calculated module cost was 4.731-4.811 US$/W. If we further extend the solid line, the module costs of Module B decrease dramatically while Module A decreases only slightly. This result revealed that the module efficiency acted as an important factor for module cost no matter which route was used for manufacturing. Improvement of the TENG efficiency and active area by upgrading precision of deposition method to further increase module efficiency is therefore an effective way to reduce the cost of Module B.

4.5.2 Levelized Cost of Electricity Produced with TENGs

The LCOE is typically used to compare system costs of electricity produced using different sources of energy. The LCOEs of traditional energy sources were 7.04–11.90 US cents/kWh, and

the costs of solar PV technologies were 9.78–19.33 US cents/kWh reported in Levelized Cost and Levelized Avoided Cost of New Generation Resources in the Annual Energy Outlook 2015. The LCOE was calculated according to Equation. (5) (Section 3), and the output was affected mainly by module cost, efficiency, and lifetime. In our module cost analysis, both Module A and B were estimated to produce TENG energy harvesting modules at a cost in the range of 0.68084-2.667 US$/W. We calculated the LCOE of a TENG energy harvesting module by assuming a module cost of 0.68084 US$/W for module A, 2.667 US$/W for module B and a lifetime of 15 years. The LCOEs were 2.569 US cents/kWh, 2.681 US cents/kWh corresponding to module efficiencies of 50%, 20% respectively for module A. And 9.198 US cents/kWh, 9.43 US cents/kWh corresponding to module efficiencies of 24%, 20% respectively for Module B, which were lower than that of traditional energy sources (Figure 19) for Module A and in the same range of wind power for Module B. Details of the calculation are shown in the Methods section and Table S10. This analysis indicates that module efficiency has a significant influence on the LCOE.

Commented [ir8]: Needs a reference

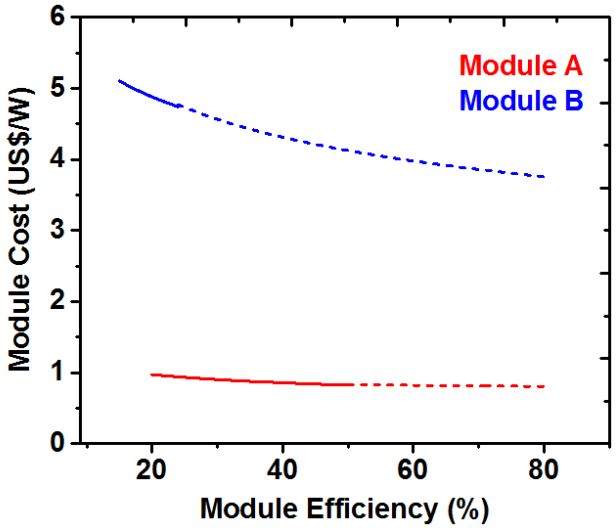

Figure 19: Module cost of TENGs as a function of module efficiency. Except for the independent variables in these Figures, the other parameters associated with Module A and Module B were fixed. The solid lines were calculated based on the range of reported efficiencies; the dashed lines are based on calculations assuming high module efficiencies that are expected but not yet achieved.

Figure 20 shows the effect of lifetime on the LCOE of TENG for wave energy harvesting. The LCOEs estimated 50% and 40% efficiency for Module A, and 24% and 20% for Module B but each decreases exponentially with the extension of the system lifetime in the range 10–30 years. For high efficiency (50%) modules, a lifetime of 10 years can lead to an LCOE of 3.42 US cents/kWh. The low-efficiency (40%) modules require a short lifetime (12-years) to achieve the similar LCOE. A conservative estimate of discount rate 5% is used above. Based on the above analysis, the module efficiency and lifetime were the most sensitive factors for the LCOE of TENGs. The ultra-low LCOE of TENGs was achieved to be 2.569–2.68 US cents/kWh with 15 years' lifetime, surpassing the United States "Sun Shot Initiative" target of 6.0 US cents/kWh. Hence, improvement of the efficiency and the lifetime of TENGs are urgent tasks from the perspective of cost, and more efforts should be devoted to this field.

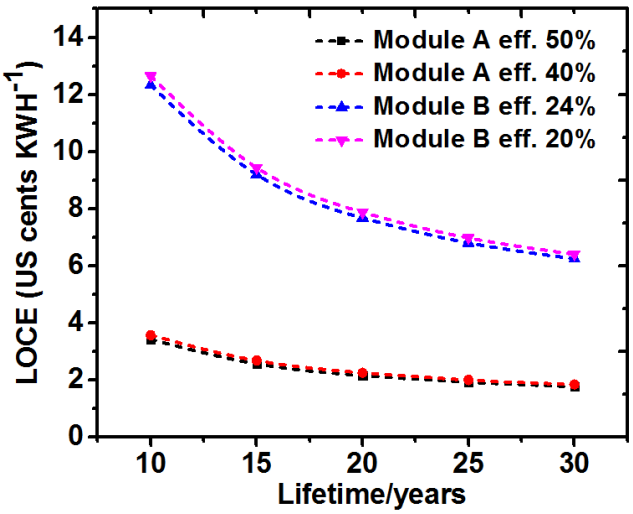

Figure 20: The relationship between LCOE and lifetime. A system lifetime <10 years was not considered in our analysis.

The LCOE is calculated according to Equation. (5) (Method part), and it is affected mostly by module cost, efficiency, and lifetime. In our cost analysis, the modules cost is estimated to be in the range of 0.68–2.667 US$/W corresponding to TENG A and TENG B, respectively. We calculated the LCOE of a TENG A by assuming a module cost of 0.68 US$/W and a lifetime of

15 years. While, TENG B is calculated by assuming a module cost of 2.667 US$/W and a lifetime of 15 years. The TENG A LCOEs are 2.569 US cents/kWh and 2.681 US cents/kWh for efficiency 50% and 40%, respectively. On the other hand, the TENG B LCOEs are 9.198 US cents/kWh and 9.43 US cents/kWh corresponding to module efficiencies of 24% and 20%, respectively, which are lower than other energy sources (Figure 21). Details of the calculation are shown in the Methods section and Table S10. Consequently, module efficiency has a significant influence on the LCOE.

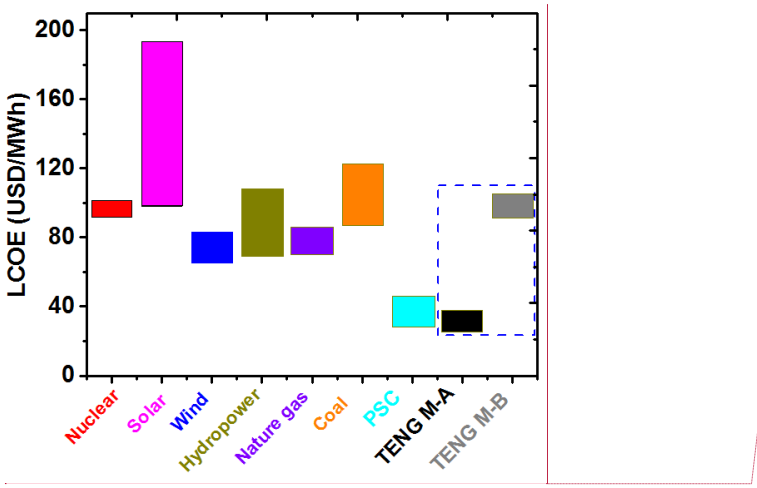

Commented [T9]: Since gold is no longer used, how the LCOE of module B is still that high? Please check

Figure 21: The comparison of LCOE based on coal, nature gas, unclear, wind, commercialized solar PV, hydropower, PSC and TENG modules. The LCOE values are referenced to the Levelized Cost and Levelized Avoided Cost of New Generation Resources in the Annual Energy Outlook 2015 reported by United States Energy Information Administration.

5. Summary and concluding remarks

Mechanical energy is available in abundant quantities everywhere around us and is completely independent of weather, day/night or even season. This abundant source of energy remains largely untapped but with continuous and improved power conversion efficiencies reported in the past few years, triboelectric nanogenerator TENGs are touted as a highly promising source of electricity generation from mechanical energy. In this paper, a cradle-to-grave life cycle assessment of two TENGs modules was performed. The life cycle environmental impact

assessment involves 11 midpoint impact categories, and an endpoint evaluation by following the Eco-indicator 99 methodology. We shed light on two important sustainability indicators and find that TENG modules have the shortest EPBT among existing PV technologies. We find that the environmental hotspots come from the use of acrylic (both modules), PTFE (module A) and FEP (module B). As such, for future development of this technology, material optimization should be advanced. Moreover, we evaluated the sustainable indicators considering the uncertainties of major input parameters. The resulting probability distributions demonstrate that for TENGs at the current stage, EPBTs are stable and competitive, while CO_2 emission factors are less stable. Lastly, through sensitivity analysis, we find that TENG modules are potentially one of the most environmentally sustainable energy harvesters if future development confirms a larger performance ratio and a longer lifetime. To this end, a comparative techno economic analysis of the TENG modules was performed based on an annual capacity of 100 MW. We found that the module costs for Module A could be much lower than other technologies when fully operational, while Module B was found to be comparable with the cost of hydropower technologies. The results of the sensitivity analysis showed that improved performance efficiency could significantly reduce module cost. The fabrication of high-efficiency modules through the adoption of high precision fabrication processes was the most promising approach for further reducing the cost. The results indicate an estimated levelized cost of Module A and B to be US 2.681 cents/kWh and US 9.43 cents/kWh, respectively. The LCOE of TENGs was also very sensitive to module efficiency and can be expected to be lower than that of other energy technologies if the module efficiency and lifetimes can exceed 25% and 15 years, respectively. To achieve these targets, more efforts should be made to improve the lifetime and efficiency of TENGs rather than to identify cheaper materials and fabrication processes.

Acknowledgements

This research was supported by KAUST and the Hightower Chair foundation. The support provided for completing this research is gratefully acknowledged.

References

1. EIA, *US Energy Information Administration, Washington, DC*, 2013.
2. IPCC, *Climate change 2014: mitigation of climate change*, Cambridge University Press, 2015.
3. Z. L. Wang, J. Chen and L. Lin, *Energy & Environmental Science*, 2015, **8**, 2250-2282.
4. D. Evans, *How the Next Evolution of the Internet is Changing Everything, Whitepaper, Cisco Internet Business Solutions Group (IBSG)*, 2011, **1**, 1-12.
5. Y. Gao and Z. L. Wang, *Nano letters*, 2007, **7**, 2499-2505.

6. Y. Qin, X. Wang and Z. L. Wang, *Nature*, 2008, **451**, 809-813.
7. X. Wang, J. Song, J. Liu and Z. L. Wang, *Science*, 2007, **316**, 102-105.
8. S. Xu, B. J. Hansen and Z. L. Wang, *Nature communications*, 2010, **1**, 93.
9. S. Xu, Y. Qin, C. Xu, Y. Wei, R. Yang and Z. L. Wang, *Nature nanotechnology*, 2010, **5**, 366-373.
10. R. Yang, Y. Qin, L. Dai and Z. L. Wang, *Nature Nanotechnology*, 2009, **4**, 34-39.
11. J. Henniker, 1962.
12. R. G. Horn and D. T. Smith, *Science*, 1992, **256**, 362.
13. R. G. Horn, D. Smith and A. Grabbe, *Nature*, 1993, **366**, 442-443.
14. Z. L. Wang and J. Song, *Science*, 2006, **312**, 242-246.
15. F.-R. Fan, Z.-Q. Tian and Z. L. Wang, *Nano Energy*, 2012, **1**, 328-334.
16. W. Tang, T. Jiang, F. R. Fan, A. F. Yu, C. Zhang, X. Cao and Z. L. Wang, *Advanced Functional Materials*, 2015, **25**, 3718-3725.
17. G. Zhu, B. Peng, J. Chen, Q. Jing and Z. L. Wang, *Nano Energy*, 2015, **14**, 126-138.
18. Z. H. Lin, G. Zhu, Y. S. Zhou, Y. Yang, P. Bai, J. Chen and Z. L. Wang, *Angewandte Chemie International Edition*, 2013, **52**, 5065-5069.
19. Z. Wen, J. Chen, M.-H. Yeh, H. Guo, Z. Li, X. Fan, T. Zhang, L. Zhu and Z. L. Wang, *Nano Energy*, 2015, **16**, 38-46.
20. H. Zhang, Y. Yang, T.-C. Hou, Y. Su, C. Hu and Z. L. Wang, *Nano Energy*, 2013, **2**, 1019-1024.
21. Y. Yang, H. Zhang, Y. Liu, Z.-H. Lin, S. Lee, Z. Lin, C. P. Wong and Z. L. Wang, *ACS nano*, 2013, **7**, 2808-2813.
22. Z. Li, J. Chen, J. Yang, Y. Su, X. Fan, Y. Wu, C. Yu and Z. L. Wang, *Energy & Environmental Science*, 2015, **8**, 887-896.
23. S. Chen, N. Wang, L. Ma, T. Li, M. Willander, Y. Jie, X. Cao and Z. L. Wang, *Advanced Energy Materials*, 2016.
24. G. Zhu, J. Chen, T. Zhang, Q. Jing and Z. L. Wang, *Nature communications*, 2014, **5**.
25. K. Y. Lee, J. Chun, J. H. Lee, K. N. Kim, N. R. Kang, J. Y. Kim, M. H. Kim, K. S. Shin, M. K. Gupta and J. M. Baik, *Advanced Materials*, 2014, **26**, 5037-5042.
26. L. Zhang, B. Zhang, J. Chen, L. Jin, W. Deng, J. Tang, H. Zhang, H. Pan, M. Zhu and W. Yang, *Advanced Materials*, 2016, **28**, 1650-1656.
27. Z.-H. Lin, G. Cheng, X. Li, P.-K. Yang, X. Wen and Z. L. Wang, *Nano Energy*, 2015, **15**, 256-265.
28. F.-R. Fan, L. Lin, G. Zhu, W. Wu, R. Zhang and Z. L. Wang, *Nano letters*, 2012, **12**, 3109-3114.
29. G. Zhu, C. Pan, W. Guo, C.-Y. Chen, Y. Zhou, R. Yu and Z. L. Wang, *Nano letters*, 2012, **12**, 4960-4965.
30. G. Zhu, Z.-H. Lin, Q. Jing, P. Bai, C. Pan, Y. Yang, Y. Zhou and Z. L. Wang, *Nano letters*, 2013, **13**, 847-853.
31. G. Zhu, J. Chen, Y. Liu, P. Bai, Y. S. Zhou, Q. Jing, C. Pan and Z. L. Wang, *Nano letters*, 2013, **13**, 2282-2289.
32. G. Zhu, Y. S. Zhou, P. Bai, X. S. Meng, Q. Jing, J. Chen and Z. L. Wang, *Advanced Materials*, 2014, **26**, 3788-3796.
33. T. Ibn-Mohammed, S. Koh, I. Reaney, A. Acquaye, D. Wang, S. Taylor and A. Genovese, *Energy & Environmental Science*, 2016, **9**, 3495-3520.
34. T. Ibn-Mohammed, R. Greenough, S. Taylor, L. Ozawa-Meida and A. Acquaye, *Energy and Buildings*, 2013, **66**, 232-245.
35. S. Hellweg and L. M. i Canals, *Science*, 2014, **344**, 1109-1113.
36. S. Koh, T. Ibn-Mohammed, A. Acquaye, K. Feng, I. Reaney, K. Hubacek, H. Fujii and K. Khatab, *Scientific Reports*, 2016, **6**, 39514.
37. A. Acquaye, K. Feng, E. Oppon, S. Salhi, T. Ibn-Mohammed, A. Genovese and K. Hubacek, *Journal of Environmental Management*, 2016, **187**, 571-585.

38. *Quadrennial Technology Review 2015, Chapter 6: Innovating Clean Energy Technologies in Advanced Manufacturing*, U.S Departmetn of Energy, 2015.
39. F. C. Krebs, *Solar energy materials and solar cells*, 2009, **93**, 394-412.
40. R. R. Søndergaard, M. Hösel, N. Espinosa, M. Jørgensen and F. C. Krebs, *Energy Science & Engineering*, 2013, **1**, 81-88.
41. G. Rebitzer, T. Ekvall, R. Frischknecht, D. Hunkeler, G. Norris, T. Rydberg, W.-P. Schmidt, S. Suh, B. P. Weidema and D. W. Pennington, *Environment international*, 2004, **30**, 701-720.
42. T. Ibn-Mohammed, R. Greenough, S. Taylor, L. Ozawa-Meida and A. Acquaye, *Building and Environment*, 2014, **72**, 82-101.
43. A. A. Acquaye, T. Wiedmann, K. Feng, R. H. Crawford, J. Barrett, J. Kuylenstierna, A. P. Duffy, S. L. Koh and S. McQueen-Mason, *Environmental science & technology*, 2011, **45**, 2471-2478.
44. D. Collado-Ruiz and H. Ostad-Ahmad-Ghorabi, *Journal of Cleaner Production*, 2010, **18**, 355-364.
45. R. García-Valverde, J. A. Cherni and A. Urbina, *Progress in Photovoltaics: Research and Applications*, 2010, **18**, 535-558.
46. N. Espinosa, M. Hösel, D. Angmo and F. C. Krebs, *Energy & Environmental Science*, 2012, **5**, 5117-5132.
47. D. Yue, P. Khatav, F. You and S. B. Darling, *Energy & Environmental Science*, 2012, **5**, 9163-9172.
48. J. J. Conti, P. D. Holtberg, J. A. Beamon, A. Schaal, J. Ayoub and J. T. Turnure, *United States of America Department of Energy Information. Office of Integrated and International Energy Analysis. Available at http://www. eia. gov/neic/speeches/newell_12162010. pdf*, 2011.
49. I. ISO, *London: British Standards Institution*, 2006.
50. I. ISO, *International Organization for Standardization, Geneva, Switzerland*, 2013.
51. A. Azapagic, C. Pettit and P. Sinclair, *Clean Technologies and Environmental Policy*, 2007, **9**, 199-214.
52. Ecoinvent, Ecoinvent database, http://www.ecoinvent.org/, (accessed 20th November 2016, 2016).
53. J. B. Guinée, *Int J LCA*, 2002, **7**, 311-313.
54. S. M. Le, *Solar Energy Techonologies Office*, U.S. Department of Energy,, 2015.
55. W. Kellogg, M. Nehrir, G. Venkataramanan and V. Gerez, *IEEE Transactions on energy conversion*, 1998, **13**, 70-75.
56. K. Branker, M. Pathak and J. M. Pearce, *Renewable and Sustainable Energy Reviews*, 2011, **15**, 4470-4482.
57. M. Le, *SUNSHOT INITIATIVE*

U.S. Department of Energy, Solar Energy Technologies Office, 2015.
58. D. L. Smith and D. W. Hoffman, *Physics Today*, 1996, **49**, 60.
59. Polyflon Technology Limited, 100 PTFE Film (Polytetrafluoroethylene), http://www.polyflon.co.uk/products/fluoropolymer-film/ptfe-film, (accessed 16th December, 2016, 2016).
60. Teflon, Fluoroplastic Film-Properties Bulletin, https://www.chemours.com/Teflon_Industrial/en_US/assets/downloads/teflon-fep-film-properties.pdf, (accessed 16th December, 2016).
61. R. Laleman, J. Albrecht and J. Dewulf, *Renewable and Sustainable Energy Reviews*, 2011, **15**, 267-281.
62. J. Gong, S. B. Darling and F. You, *Energy & Environmental Science*, 2015, **8**, 1953-1968.